Molecular Dynamics Simulations of a K Channel Model: Sensitivity to Changes in Ions, Waters, and Membrane Environment

Charlotte E. Capener and Mark S. P. Sansom*

Laboratory of Molecular Biophysics, Department of Biochemistry, Rex Richards Building, University of Oxford, South Parks Road, Oxford, OX1 3QU, U.K.

Received: August 2, 2001; In Final Form: December 17, 2001

Biological ion channels are protein pores of sub-nanometer radius that enable rapid movement of selected ions across membranes. K channels are selective for K^+ over Na^+ ions, a function that resides in a narrow selectivity filter at the extracellular end of the channel. A model of an inward rectifier (Kir), derived from the structure of the bacterial channel KcsA, has been used in multi-nanosecond MD simulations to explore the conformational dynamics of the channel under different simulation conditions. Different simulation conditions were compared: a lipid bilayer vs a membrane-mimetic octane slab, different numbers of water molecules in the central channel cavity, and K^+ vs Na^+ ions in the selectivity filter of the channel. Structural drift from the initial model was small, and there was little effect of simulation conditions on this drift. In a long (10 ns) simulation it was shown that significant conformational changes were restricted to the water-exposed loops while the core transmembrane structure remained unchanged. A flexibility gradient was observed in the channel molecule along the channel axis, with flexibility increasing from the extracellular to the intracellular end. This correlates with biological function, ion selectivity being located in the filter at the extracellular end of the molecule, whereas gating is thought to be located at the intracellular mouth of the channel. Examination of the dynamics of ions and water molecules in the filter revealed relaxation of the K^+-water-K^+ single file to a preferred 0101 configuration on a 1 ns time scale. On a longer (10 ns) time scale K^+ ions were seen to fully traverse the filter, and to exit/reenter relative to the central cavity. The filter was shown to be flexible, both in terms of fluctuations in its radius profile and in terms of local changes in conformation in response to ion translocation. Na^+ ions resulted in a narrowing of the filter compared to K^+ ions. Na^+ ions occupied slightly different sites in the filter, and exhibited octahedral coordination (four filter oxygens + two water oxygens) rather than the cubic coordination (by eight filter oxygens) preferred by K^+ ions.

1. Introduction

Pores of sub-nanometer dimensions are of importance in chemistry[1−4] and biology,[5,6] e.g., as channels through biological membranes. A biological channel consists of a pore ca. 3 nm long and of minimum radius ca. 0.1−0.3 nm that spans a lipid bilayer membrane. Ion channels are integral membrane proteins allowing the rapid movement of ions down their electrochemical gradients across cell membranes.[7] Such channels are usually "selective", i.e., only certain ions are permitted to flow through the central pore. Understanding the physicochemical basis of channel function is a topic of some complexity[8−17] requiring contributions from structural biology, physical chemistry, and molecular simulations.

An X-ray crystal structure provides an essentially static picture of a membrane protein. However, understanding dynamics is essential to a full description of the physical events underlying ion transport. Computer simulations are of some use in this context. In particular, molecular dynamics (MD) simulations have been successfully applied to study membrane proteins in general,[18] and ion channels in particular.[19−22] For example, previous simulation studies[23−26] suggest that ion channels exhibit a degree of flexibility, rather than acting as a rigid tube through which selected ions pass. This is supported by recent experimental structural studies.[27]

Potassium channels are a large family of ion channels that play an important role in the membrane physiology of cells, and share a common property of selectivity for K^+ over Na^+ ions.[7] This selectivity is associated with a conserved sequence motif TVGYG found in the selectivity filter of the pore-forming region of the protein. Simpler K channels, such as the bacterial channel KcsA[28] and the inwardly rectifying K channel family (the Kir channels, the subject of this paper),[7,29] are formed from a tetramer, each subunit of which provides two transmembrane helices M1 and M2 between which is a P loop containing the selectivity filter. The X-ray structure of KcsA[30] revealed that the P loop was made up of a descending P helix and an ascending filter region in an extended conformation. Four ion-binding sites (S1 to S4) are formed by rings of oxygen atoms from the ascending loop oriented toward the pore center to form the selectivity filter. These oxygen atoms effectively replace the hydration shell of water lost on entry of the ion into the narrow filter.[27]

Kir6.2 is a member of the Kir channel family and is present in the pancreatic β-cell where it plays a role in regulation of insulin secretion.[31] It is weakly K^+ selective, with a permeability ratio of $P_{Na}/P_K = 0.39$ for internal Na^+ relative to K^+ ions.[32] In the absence of an X-ray structure for Kir6.2, a homology model based on the structure of KcsA has been generated.[33] Sequence identity between Kir6.2 and KcsA is relatively high in the pore region (∼30%) despite being low overall (∼15%),

* To whom correspondence should be addressed. Fax: +44-1865-275182. Phone: +44-1865-275371. E-mail: mark@biop.ox.ac.uk.

10.1021/jp0129986 CCC: $22.00
Published on Web 03/26/2002

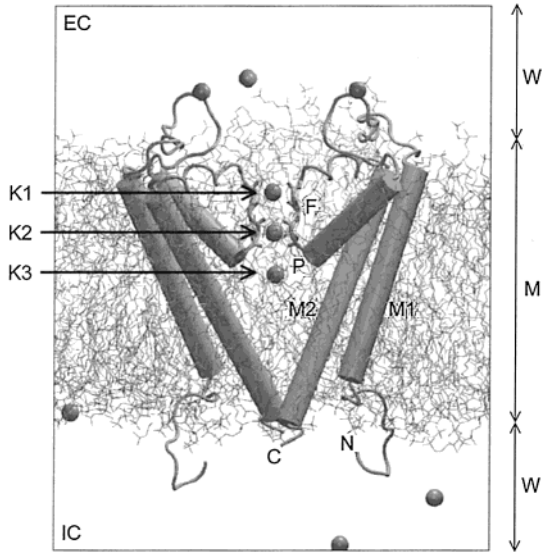

Figure 1. Representation of the Kir6.2 channel homology model, shown as cylinders (for α-helical regions) and loops, with the carbonyl oxygens of the selectivity filter (F) as bonds. For clarity, only two of the four subunits that make up the channel are shown. They are embedded in a phospholipid bilayer. K^+ ions are shown as spheres, their initial locations within the channel labeled K1, K2, and K3. The extent of the water (W) and membrane (M) regions are indicated, as are the intracellular (IC) and extracellular EC) faces of the membrane. The N-terminus (N), C-terminus (C), the M1 and M2 helices, and the P helix are also labeled.

suggesting that the assumption of a shared architecture for the central pore-forming domain is reasonable.[34] This assumption is supported by recent experimental studies in which the KcsA pore was "transplanted" into the nonmembrane domains of a Kir channel and shown to retain its function.[35]

In this study we use MD simulations to investigate aspects of the structural dynamics of the Kir6.2 channel model. The Kir6.2 homology model is embedded in either a solvated phospholipid lipid bilayer or a bilayer mimetic (octane) slab. We analyze the dynamics of the protein in relationship to the nature of the simulation conditions. This extends a preliminary simulation[33] study that did not explore sensitivity to simulation conditions. In particular, we examine the structural dynamics of the selectivity filter: in long (10 ns) MD simulations, in response to changes in ionic species (K^+ vs Na^+), and in response to different treatments of long-range electrostatic interactions (cutoff vs PME) in the simulations. The results suggest that the structural dynamics of the filter are sensitive to the nature of the ion (K^+ vs Na^+) but are somewhat less sensitive to other changes in the simulation conditions.

2. Methods

The overall aim of this study was to investigate the dependence of MD simulations of a K channel model (see Figure 1) on various aspects of the simulation setup. These included the species (K^+ or Na^+) of ions in the pore, the number of water molecules in the cavity region of the pore, the environment (lipid bilayer vs octane slab) of the protein, and the treatment of long-range electrostatics (see below). The resultant simulation systems are summarized in Table 1. Each of the systems was energy minimized prior to MD simulation in order to relax any steric conflicts generated during setup of the system. Then, a restrained MD run was performed on the system. During this, the protein and the cations within the pore were restrained to their initial locations, while the rest of the system (water and lipid or octane) remained free to relax around the protein. Finally, an unrestrained MD simulation was performed for each simulation.

2.1. Channel Model. The model of Kir6.2 used in the simulations was that described in ref 33. It includes 118 residues corresponding to the central pore-forming domain aligned with the KcsA structure. Fifty-seven residues at the N-terminus and 215 at the C-terminus are missing. The model was generated using Modeller v4[36] using the KcsA crystal structure as the template. Four-fold rotational symmetry was imposed during the modeling procedure, as were secondary structure restraints to ensure the M1 and M2 regions were α-helical.

Protein side chain charges for ionisable residues were adjusted to agree with pK_A calculations. The latter were performed as previously described[33,37,38] using UHBD version 5.1.[39] These calculations were performed with $3K^+$ ions located within the channel at sites corresponding to those found in the X-ray structure of KcsA, i.e., two K^+ ions in the filter and one ion in the cavity.

In the (closed state) Kir6.2 model, the pore region is closed off at the intracellular end to form a discrete cavity whose water molecules are unable to exchange with those of the bulk region. As with KcsA simulations,[23,25,40] the question of how many waters can be accommodated within the cavity is one of some interest, as it is conceivable that the number of cavity water molecules may influence, for example, the behavior of the ions in the filter. In our preliminary simulations[33] the cavity was solvated by overlaying the protein plus lipid coordinates with an equilibrated box of SPC waters and then eliminating those waters that overlapped with a nonwater atom. This yielded 13 waters in the cavity (simulation K3W13). However, we had some concern that this procedure may have undersolvated the cavity. The program HOLE[41] was used to estimate the cavity volume. This suggested that there should be 20 molecules in the cavity if one assumes that the density of waters in the cavity is equal the bulk density of water. However, this latter assumption may not be correct.[42] We therefore explored a Monte Carlo procedure for water insertion into the cavity using the program MMC[43] (see http://inka.mssm.edu/~mezei/mmc/). This also suggested that the cavity was capable of accommodating up to 20 water molecules. Thus, a number of simulations (see Table 1) used 20 waters within the cavity.

Three cations (K^+ or Na^+) were placed within the channel in each simulation, two in the filter and one in the central cavity. In Kir6.2 the filter sequence is $T^{130}IGFG^{134}$. The four ion binding sites are defined as follows: S1 is formed by carbonyl oxygens from F133 and G132, S2 is formed by carbonyl oxygens from G132 and I131, S3 is formed by carbonyl oxygens from I131 and T130, whereas S4 is formed by carbonyl oxygens from the T130 mainchain plus hydroxyl groups from the T130 side chains. In each simulation the two filter ions were placed in sites S1 and S3. The cavity K^+ ion was positioned by replacing a water molecule within the cavity. There were also 11 K^+ ions, positioned randomly in the bulk water regions, to maintain overall electrical neutrality of the simulation system.

2.2. Simulations. For the bilayer simulations, the Kir6.2 models were embedded in a preequilibrated POPC bilayer using the methods described in ref 33 and solvated with SPC[44,45] waters, using ca. 45 waters per lipid molecule to ensure complete solvation of the bilayer. For the octane simulation, the Kir6.2 model was solvated in an octane slab of thickness ca. 4.5 Å. This was equilibrated using restrained molecular dynamics where the protein was fixed, and the octane was allowed to relax around it until the system density had stabilized.

TABLE 1: Summary of Simulations[a]

simulation	filter	cavity	membrane	cutoff or PME?	waters	atoms	Cα-RMSD at 1 ns (Å)	Cα-RMSD at end (Å)	time (ns)
K3W13	$2K^+ + H_2O$	$K^+ + 13H_2O$	POPC	C/O	11721	51981	2.5	3.2	10
K3W20	$2K^+ + H_2O$	$K^+ + 20H_2O$	POPC	C/O	11742	52050	2.7	3.0	5
K3OCT	$2K^+ + H_2O$	$K^+ + 20H_2O$	octane	C/O	10827	44005	3.1	5.0	10
Na3W20	$2Na^+ + H_2O$	$Na^+ + 20H_2O$	POPC	C/O	11742	52050	2.3	2.6	2
K3PME	$2K^+ + H_2O$	$K^+ + 20H_2O$	POPC	PME	11741	52047	2.4	2.4	1

[a] Summary of the five simulations of Kir6.2 described in this paper. Long-range electrostatic and van der Waals forces were approximated by either cutoff (C/O) or particle mesh Ewald (PME) methods. Cα-RMSD refers to the root-mean-square deviation of the Cα atoms from their initial positions after 1 ns of simulation time and at the end of the simulation.

Molecular dynamic (MD) simulations were run using Gromacs v2.0 (see http:// www.gromacs.org). The LINCS algorithm[46] was used to constrain bond lengths. The time step was 2fs. NPT (i.e., constant number of particles, temperature, and pressure) conditions were applied, with a constant pressure of 1 bar maintained independently in all three directions via a coupling constant of $\tau p = 1.0$ ps.[47] In the octane simulations pressure coupling was applied only in the *z* direction, with the *x* and *y* dimensions of the simulation box remaining fixed as in ref 48. Water, lipid, and protein were coupled separately to a temperature bath at 300 K with a coupling constant of $\tau_T = 0.1$ ps. Lipid parameters were based on those used in MD studies of DPPC,[49,50] with the addition of some GROMOS parameters for the double bond in the oleoyl tail. Octane parameters were from GROMOS96.[45] Lipid−protein interactions also used GROMOS parameters. The K^+ parameters were as in ref 51 and have been used in MD simulations of KcsA.[25] Na^+ parameters were provided within Gromacs.[51] Twin-range cutoffs were used for long-range interactions, set at 10 Å for van der Waals interactions and 17 Å for electrostatic interactions. MD simulations were performed on a SGI Origin 2000, typically taking ca. 21days of CPU time per ns on a single 195 MHz R10000 processor.

Structural diagrams were prepared using Molscript[52] and Raster3D.[53] Pore radius profiles were calculated using HOLE.[41] Secondary structure analysis used DSSP.[54] Other analyses used GROMACS and/or locally written code.

3. Results

The aim of these simulations is to examine the conformational dynamics, on a 1 to 10 ns time scale, of a Kir6.2 model as a function of simulation conditions. In particular, we are interested in the overall stability of the backbone fold, and in the conformation of the filter in response to the species of the cations within it. The latter is of particular interest given the measurable permeability of Kir6.2 to Na^+ ions in addition to the preferred K^+ ions.

3.1. Drift from Initial Structure. A measure of the conformational stability of a model is provided by the drift from its initial structure over the course of a simulation. This may be measured via the root-mean-square deviation (RMSD) of the Cα atoms (i.e., one atom per amino acid residue) from their initial coordinates. By focusing on the Cα coordinates one focuses on the overall fold of the molecule, rather than, for example. local changes in side chain conformations. In Table 1 the Cα RMSDs after 1ns are compared for the five simulations, and in Figure 2 Cα RMSDs are plotted as a function of time for three of the simulations.

From Table 1 it can be seen that after 1 ns the Cα RMSDs are all ca. 2.5 Å, with the exception of that for K3OCT which is a little greater than 3 Å. Values of ca. 2 to 2.5 Å have been seen for comparable simulations of membrane proteins (including KcsA,[25] porins,[55] and GlpF[56]) that started with X-ray crystal

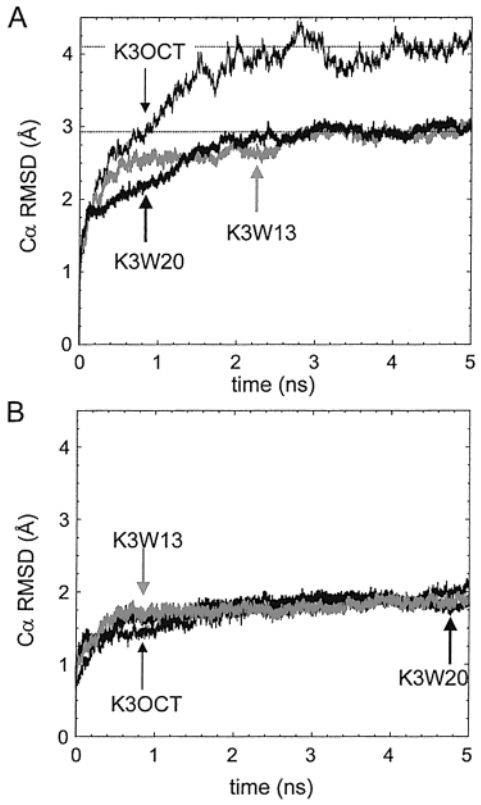

Figure 2. Drift from the initial model. **A** The Cα atom root-mean-square deviations (RMSDs) for all residues of the model are shown vs time for three simulations: K3W13 (first 5 ns only; thick gray line), K3W20 (thick black line), and K3OCT (first 5 ns only; thin black line). The dotted horizontal lines show the final RMSDs. **B** Cα atom RMSDs are shown for the same three simulations, but only for the core secondary structures residues, i.e., for the region defined by the M1 helix, the P-helix plus filter, and the M2 helix combined.

structures of the protein rather than a homology model. In all of the Kir6.2 simulations there was a steep increase in the Cα RMSD at the beginning of the simulation that generally seemed to plateau after ca. 0.5 ns. The only exception was the K3OCT simulation, for which the Cα RMSD reached a plateau of ca. 3.8 Å after ca. 2 ns.

This comparison is extended over 5 ns for three simulations (K3W13, K3W20 and K3OCT) as shown in Figure 2A. There is not any difference in the drift for the K3W13 and K3W20 simulations over 5 ns indicating that the number of water molecules in the cavity did not influence the overall conformational stability of the protein model. The cavity did not appear to collapse at all in the K3W13 simulation (using a pore radius profile[57,58] calculation to evaluate this) In both of these simulations the drift reached a plateau (of ca. 0.29 nm) after about 3 ns. In the case of K3OCT the Cα RSMD was significantly larger than for the lipid bilayer simulations, reaching a plateau of ca. 0.4 nm after 3 ns. This may be because

the octane slab is considerably more fluid than the POPC bilayer.[59] However, it may indicate also that lipid headgroups are needed to stabilize the protein conformation as discussed in the review by.[18] For example, many membrane proteins (including the Kir6.2 model) have bands of aromatic side chains at the region on their surface that corresponds to the membrane/water interface, and it is thought that interactions of such side chains with the interface may help to stabilize the protein structure in the membrane.[60,61]The latter interpretation is supported by restricting the examination of the structural drift to only the transbilayer elements (ie. the M1 and M2 helices plus the P helix and filter). When Cα RMSDs are compared for just these regions (Figure 2B), there is no difference between the three simulations, all of which reach ca. 2 Å after 5 ns. Thus the differences seem to reflect mainly the behavior of the loop regions that project out of the membrane core into the interfacial and aqueous regions.

3.2. Longer Time Scale Simulation. For the K3W13, and K3OCT simulations we explored the conformational drift out to 10 ns in order to see whether significant changes were observed on a longer time scale in a simulation of the Kir6.2 model in a lipid bilayer. For, for example, K3W13 at 1 ns, the Cα RMSD was ca. 2.5 Å; after 5 ns this had increased to ca. 3.0 Å and after 10 ns ca. 3.2 Å. Thus, 10 ns seems to be sufficient to fully explore the major component of any protein conformational change in these simulations.

It is also of some interest to examine in more detail the drift for different structural elements of the protein in, for example, K3W13. For this analysis the protein was divided into six regions: the N-terminus (residues D58 to P69), the M1 helix (H70 to A94), the turret (i.e., the M1-P loop, F95 to S113), the P helix plus the filter (I114 to P143), the M2 helix (L144 to M169), and the C-terminus (K170 to H175) (noting that residues 1−58 and 176 onward of the protein are omitted from the homology model). The fit was to all Cα atoms. The largest drifts are, as expected, in the nonhelical regions of the protein. Thus, the N-terminal region shows the largest Cα drift, ca. 5 Å in K3W13 after 10 ns (Figure 3). This may be a result of the missing N-terminal residues which may anchor the N-terminal region to the bilayer (as is the case in, for example, KcsA[62]) and make such large-scale distortions more difficult. In the turret the drift is ca. 4 Å after 5 ns or more. This loop region is in bulk water and so may be inherently more flexible than the transmembrane elements. Also the homology model of this loop is somewhat more speculative as it is 10 residues longer in Kir6.2 than in KcsA. The C-terminal region exhibits a Cα RMSD of similar magnitude to for the N-terminus. Again the lack of a complete model (215 C-terminal residues are not included) is presumed to enhance the flexibility of this region.

In contrast with the water-exposed loops, the transmembrane regions (M1, P+F, M2: see Figure 1) exhibit significantly smaller drifts. In K3W13 after 10 ns (Figure 3) the Cα RMSDs are ca. 2, 2.5, and 1.5 Å for M1, P+F, and M2, respectively. Furthermore, there are no stepwise jumps in the RMSDs, again indicating conformational stability.

3.3. Fluctuations Relative to Average Structure. In analysis of the drift from the initial structure, it is evident that the overall Cα RMSD is often dominated by an initial "relaxation" of the protein during the first ca. 0.5 ns. To explore relative mobility of different regions within a structure it is informative to evaluate the time-averaged root-mean-squared fluctuations of the Cα backbone. Such analysis reveals significantly larger fluctuations in the turret (M1-P) loop region than in the rest of the protein (data not shown). The RMSF values also provide evidence of

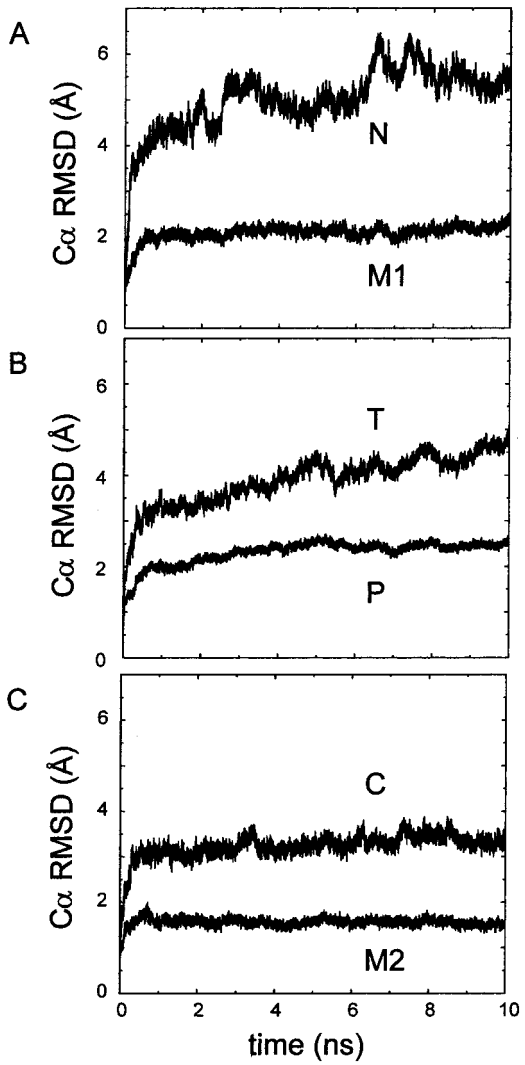

Figure 3. Cα RMSDs vs time for the whole 10 ns duration of simulation K3W13. In each case, two lines are shown corresponding to two regions of the protein structure: (A) N-terminus (N) and M1 helix (M1); (B) turret (T) and P-helix plus filter region (P); (C) M2 helix (M2) and C-terminus (C). In each case the Cα RMSD for a single structural element relative to the entire Cα starting structure is shown.

flexibility within the M2 helices, which can be seen to exhibit some hinge-bending motions around the G156 residue located roughly in the center of the transmembrane region.[63] This is particularly noticeable in the octane simulation, consistent with a lower viscosity of octane compared to that of the phospholipid bilayer enabling amplified motions of the protein to occur.

A more global view of such fluctuations may be obtained by plotting Cα RMSF values against the *z*-coordinates of the Cα atoms (Figure 4). This reveals a consistent pattern of flexibility between different simulations. First, the flexibility is evidently higher for those regions outside the membrane relative to those regions within the membrane (as noted above). More subtly, within the transmembrane region there seems to be a flexibility gradient whereby fluctuations at the extracellular end of the region (i.e., around the filter) are somewhat less than those at the opposite, intracellular end. This has also been noted in simulations of KcsA.[17,23] This flexibility gradient may reflect spatial segregation of function within K channel molecules. The filter end, exhibiting lower flexibility, is responsible for ion selectivity, whereas the opposite end of the molecule is thought to correspond to the main "gate" which switches conformation

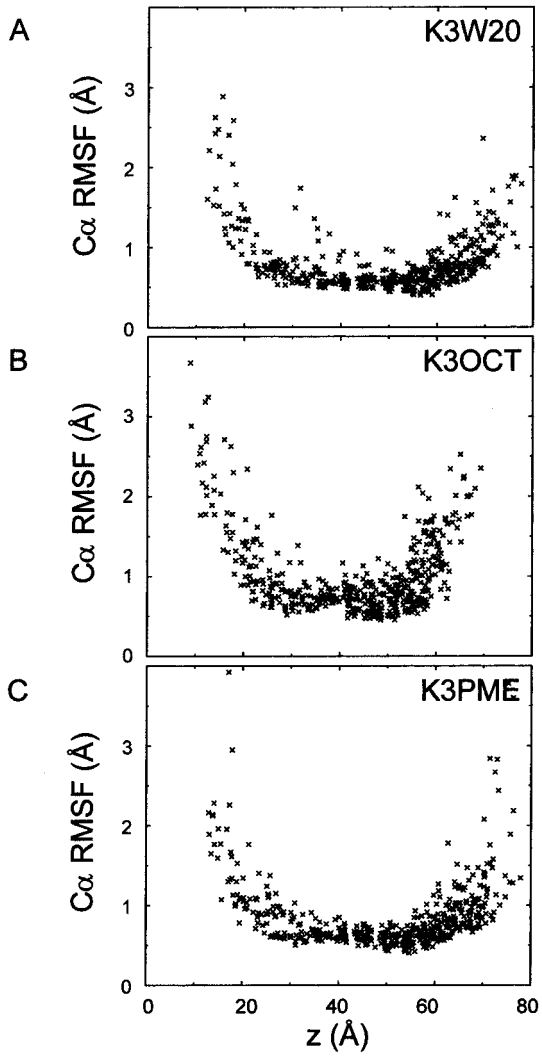

Figure 4. Cα RMSFs shown as a function of the *z* coordinate of the Cα atom for simulations: (A) K3W20, (B) K3OCT, and (C) K3PME. The membrane extends from *z* ca. 30 Å to ca. 60 Å.

between a closed and open form to control flow of ions through the channel.[64,65]

3.4. Relaxation of Ions and Water in the Filter. Let us now focus in more detail on events at the filter. In particular, we are interested to see how K^+ ions "relax" within the filter on a nanosecond time scale, and to compare the behavior of K^+ ions with that of Na^+ ions.

Motion of K^+ ions and water through the filter can be followed by tracking their *z*-coordinates vs time (Figure 5). In all of the simulations the initial locations of the two ions in the filter were at sites S1 and S3, with a water molecule at site S2. In all of the simulations, ion1 moved from S1 to S2, and ion2 from S3 to S4. In all simulations the two ions and the water molecule between moved in a more-or-less concerted single-file fashion through the selectivity filter. In the two simulations illustrated in Figures 5 and 6 this occurs right at the start of the simulation; in other simulations it occurs at a later stage. This change can be described (see ref 21) as from a 1010 to 0101 configuration of the filter (where 1 indicates the site is occupied by an ion and 0 indicates that it is not). This would suggest that the more stable configuration of the Kir6.2 filter (at least on a nanosecond time scale) is with ions at S2 and S4.

Careful examination of the *z*-trajectories for the Na3W20 simulation (Figure 5B) suggests a significant difference from the simulations with K^+ ions. In particular, ion Na2 seems to

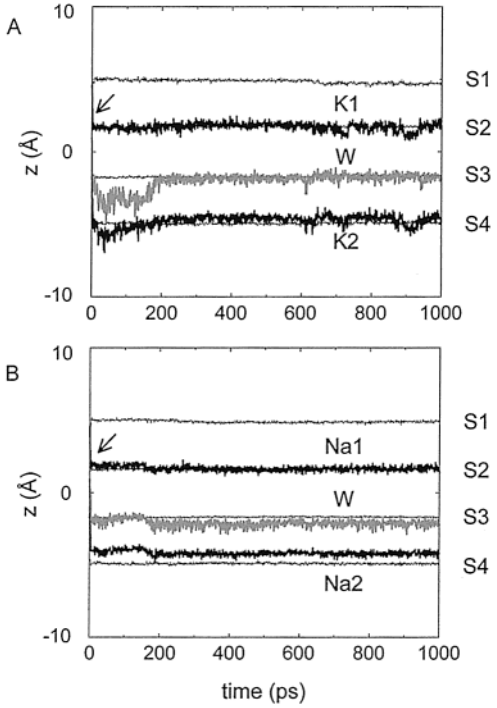

Figure 5. *z*-trajectories of ions and water relative to the selectivity filter. The thin black horizontal lines indicate the locations of the 4 sites within the filter. The thick black lines indicate the positions of the cations within the filter, and the gray lines the position of the water molecule between the two cations. Trajectories are shown for simulations (A) K3W20 (for K^+ ions K1 and K2 plus the intervening water W) and (B) Na3W20 (for Na^+ ions Na1 and Na2 plus the intervening water W). In both cases the cations were initially at sites S1 (K1 and Na1) and S3 (K2 and Na2) and the water at site S2, but rapid relaxation of the system occurred (shown by the arrows).

sit a little "above" (i.e., within the filter) site S4, interacting more strongly with the carbonyl groups of the T residue backbone than with the hydroxyls of the T side chains. The implications of this are discussed below.

3.5. Filter Flexibility and Deformation. Examining snapshots of the filter regions during the course of the simulations (Figure 6) reveals that the filter undergoes small (ca. 0.5 Å) changes in conformation as the ions and water move through it. Indeed, analysis of the pore radius profiles shows that the starting structure is not large enough to accommodate passage of K^+ ions, being ca. 0.7 Å at the narrowest part of the filter (between S2 and S3) relative to a Pauling radius of 1.33 Å for an unhydrated K^+ ion. However, the pore radius profile does fluctuate as a function of time, this being further evidence of a degree of flexibility in the filter region of the protein. Examination of the RMSF of atoms within the filter suggests that the extracellular end of the filter may exhibit somewhat greater flexibility than the intracellular end (data not shown).

A further indication of the filter flexibility is given by looking at changes in filter torsion angles vs time. Such analysis indicates that relatively large changes in backbone torsion (ϕ,ψ) angles are possible even within the confined structure of the selectivity filter. By plotting ϕ or ψ separately against time it is possible to verify that large changes in the torsion angles occur at times when an ion or water is moving from one site to another. This reinforces the idea of flexibility of the filter playing an important role in the permeation process.

Comparison of the pore radius profiles for simulations K3W20 and Na3W20 (Figure 7) reveals an overall narrowing of the filter in the latter case. Thus, the filter is able to "condense" about the smaller Na^+ ions, reducing the minimum

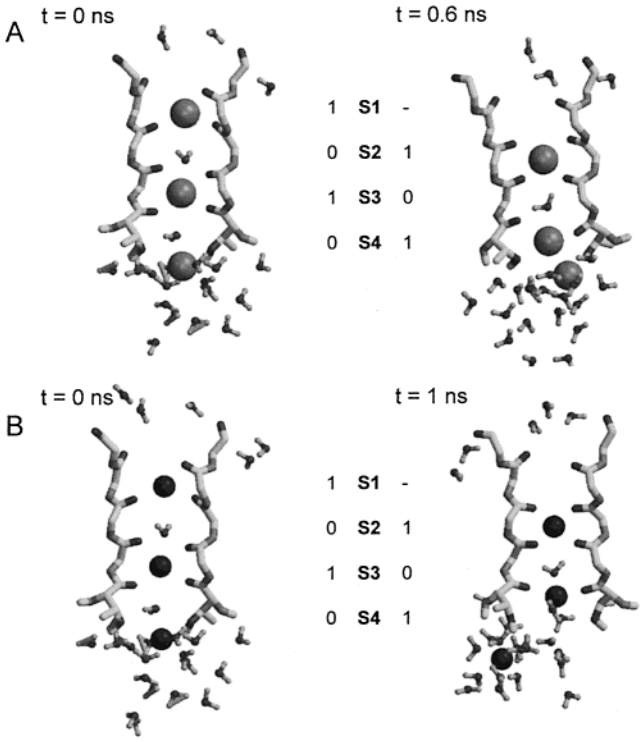

Figure 6. Snapshots of the selectivity filter with ions and water molecules during simulations. Only two of the four subunits are shown (for clarity). Simulations: (A) K3W20, $t = 0$ and 0.6 ns; (B) Na3W20, $t = 0$ and 1 ns. The backbone of the peptide plus the T side chains are shown as "bonds", selected water molecules as "ball-and-stick", and cations as spheres. S1, S2, S3, and S4 refer to the "sites" within the filter. Thus, 1010 indicates a cation at site S1, a water at S2, a cation at S3 and a water at S4.

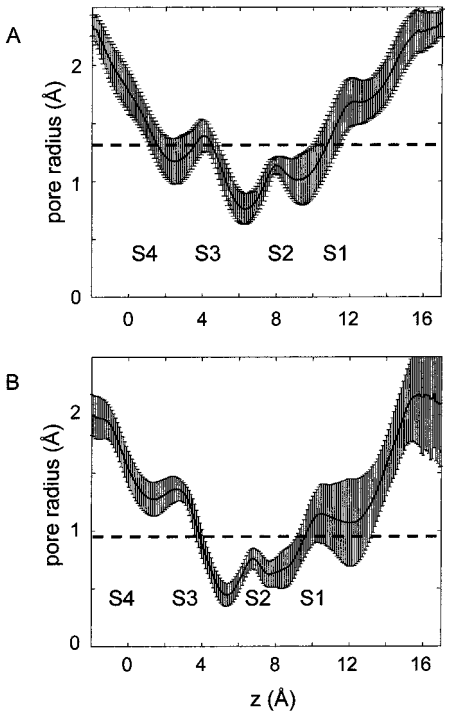

Figure 7. Pore radius profiles for simulations (A) K3W20 and (B) Na3W20. The solid curve shows the average pore radius profile within the filter region (which extends here from z ca. 0 to 12 Å). The vertical bars indicate mean ±SD (over 1 ns). The broken horizontal lines correspond to the Pauling radii of a K^+ ion (in A) and of a Na^+ ion (in B).

radius to ca. 0.5 Å. This is somewhat different from the original "rigid fit filter" model proposed by.[30]

3.6. Treatment of Long-range Electrostatics. There is some discussion of the optimal fashion in which to treat long-range electrostatics interactions in MD simulations of membrane proteins. Full pairwise Coulombic treatment for all possible pairs of atoms is not feasible for systems of ca. 40000 atoms. The simplest approximation is to use a cutoff distance, e.g., 17 Å, beyond which such interactions are discarded as negligible. However, this may introduce artifacts by omitting the cumulative effect of numerous weak long-range interactions. It has been suggested that use of Particle Mesh Ewald (PME; refs 66 and 67) may be a better approximation for membrane simulations.[68] However, for simple peptide α-helical simulations, PME has also been shown to be capable of introducing artifacts.[69] We were therefore interested to compare the results of the K3W20 simulation (above) with the same system run using PME (i.e., K3PME; see Figure 8).

Broadly, the K3PME results look very similar to the K3W20 results. The Cα RMSD after 1 ns (Table 1) is perhaps a little lower than that for K3PME, but examination of the Cα RMSDs vs time does not suggest that this is a significant difference. Examination of snapshots of the filter region (Figure 6A vs Figure 8A) does not suggest any difference: in both cases the preferred locations of the two K^+ ions appear to be S2 and S4 (Figure 5 vs Figure 8B), and small changes in the conformation of the filter backbone can be seen to occur. Thus, for this particular system we cannot see any obvious difference (on a nanosecond time scale) between cutoff and PME simulations.

3.7. Exit (and Reentry) of the Filter K^+ Ions. The pore radius profiles and potassium ion trajectories based on the 1 ns

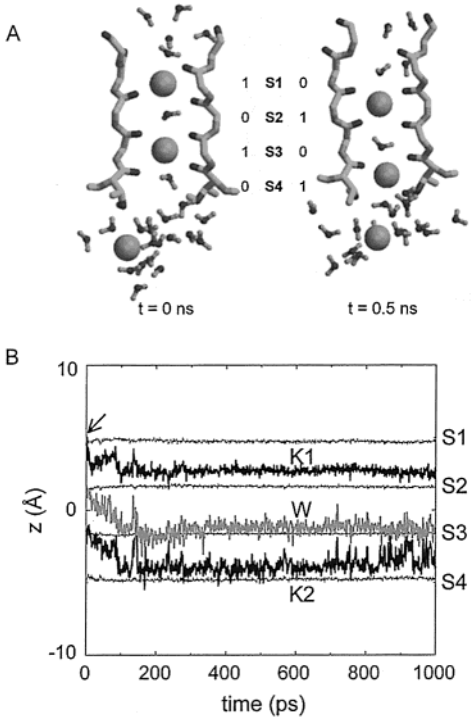

Figure 8. Simulation K3PME. (A) Snapshots of the selectivity filter with ions and water molecules during simulation. (B) *z*-trajectories of ions and water relative to the selectivity filter. The potassium ions were initially at sites S1 (K1) and S3 (K2) and the intervening water (W) at site S2, but rapid relaxation of the system occurred (shown by the arrow).

simulations reveal a degree of ion mobility within the filter, coupled to dynamic fluctuations in the filter geometry. However, to be sure that the channel model presented is consistent with

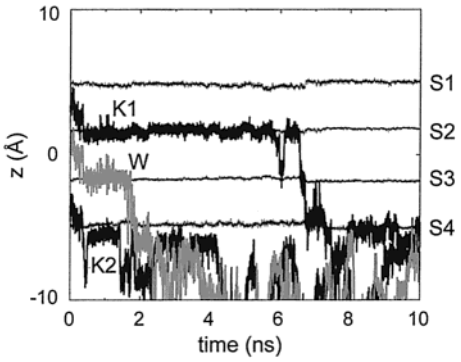

Figure 9. Extended (10 ns) *z*-trajectories of ions and water relative to the selectivity filter for simulation K3OCT. The potassium ion initially at site S1 (K1) moves to S2 (at ca. 0.5 ns) and subsequently to S3 (at ca. 6.0 and 6.8 ns) and to S4 (at ca. 7 ns) before leaving the filter at ca. 7.5 ns. K2 is initially at site S3, moves to S4 (at ca. 0.5 ns), leaves the filter (at ca. 1.5 ns) and then reenters at S4 (at ca. 8 ns). Only one water molecule, that initially at S2 (W), is shown (for clarity).

movement of ions right through the filter we examined the K^+ ion (and intervening water) trajectories in more detail for one of the 10 ns simulations (K3OCT; see Figure 9). In this trajectory we see a complex sequence of occupancy of the filter. Recalling that the initial configuration may be described as 1010 (i.e., K1 at S1, and K2 at S3), the sequence is 1010, 0101, 0100, 0101, 0100, 0010, 0101, 0010, 0001, 0000, and 0001. Thus during 10 we observe (i) movement of K1 through all four filter sites followed by exit from the filter, (ii) movement of both ions in both directions along the filter axis, and (iii) entry/exit of the filter via exchange between site 4 and the cavity. This occurs on a time scale (10 ns) consistent with that of permeation through the channel as measured electrophysiologically.

3.8. Ion Coordination: K^+ vs Na^+. Kir6.2 has a measurable permeability to Na^+ ions, such that $P_{Na}/P_K = 0.39$ to internal Na^+. It is therefore reasonable to compare the behavior of K^+ vs Na^+ ions within the Kir6.2 model filter, while realizing that a component of the ion selectivity will arise from different dehydration energies of K^+ and Na^+.[21,70,71] We have already noted that the presence of Na^+ ions seems to result in a degree of condensation/compression of the filter around the smaller ions. Here we are concerned with the coordination of K^+ vs Na^+ ions within the filter (Figure 10). First coordination shells were defined as O atoms within a cutoff distance of 3.2 Å for K^+ vs 2.5 Å for Na^+ on the bases of maximum observed cation−oxygen distances within crystals.[72] There is clearly a difference in coordination between K^+ and Na^+. At S2, the average coordination number of K^+ is ca. 7, whereas for Na^+ it is ca. 5. At site S4 the figures are 5 and 4, respectively. These should be compared with coordination numbers of K^+ ca. 8 and Na^+ ca. 6 in bulk solution determined by NMR spectroscopy[73] and of ca. 8 and ca. 6 for K^+ and Na^+, respectively, in KcsA simulations.[74]

In light of these analyses, one may reexamine the snapshots from the K3W20 and Na3W20 simulations (Figure 6), and the trajectories of the ions for the same simulations. In combination with the coordination number results these would suggest that the main difference between K^+ and Na^+ ions in the filter is at site S4, where the K^+ ion is coordinated in a loose cubic fashion, by the 4 T carbonyls plus 4 T hydroxyl oxygens, whereas the Na^+ ion is coordinated approximately octahedrally, the strongest interactions being with four T carbonyl oxygens. It is tempting to suggest that such differences may correlate with the lower permeability for Na^+ than for K^+.

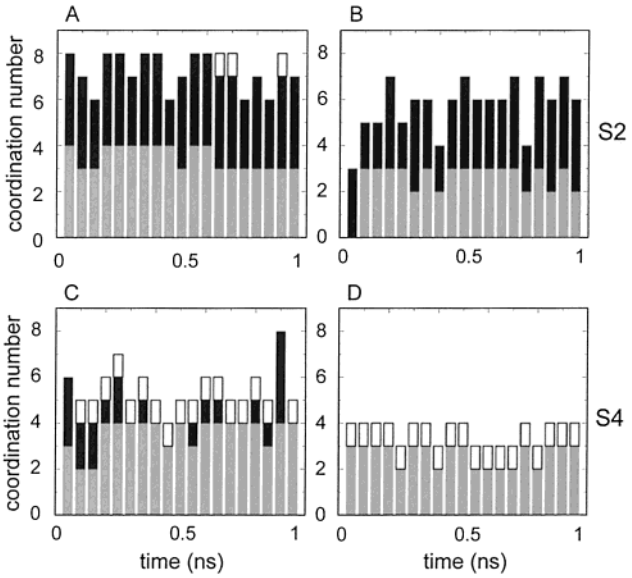

Figure 10. Coordination numbers for simulations: (A), (C) K3W20, (B), (D) Na3W20. (A) shows the coordination number of K1 and (B) that of Na1. The gray bars correspond to the CO group of residue G and the black bars to the CO group of residue I in the filter (sequence TIGY) region. The white bars correspond to water. (C) shows the coordination number of K2 and (D) that of Na2. The gray bars correspond to the CO group of residue T and the black bars to the side chain hydroxyl oxygen of residue T in the filter.

4. Discussion

4.1. Evaluation of Simulation Studies. The results described above provide some evidence that MD simulations of aspects of potassium channel behavior are quite robust to various changes in the setup of the system. By direct comparisons between the simulations we are able to assess the effects of altering certain conditions.

1. Longer Simulations and Lipid Bilayer vs Octane. It is known that the time scale of lipid motion is slow, with phospholipid dihedral transitions in the headgroup area taking of the order of hundreds of picoseconds, and lateral motions of lipids within the bilayer requiring times of the order of nanoseconds. In contrast, the dynamics of a membrane mimetic octane slab are orders of magnitude faster.[59] Remembering that we are starting with a homology model rather than a crystal structure, we were sensitive to the possibility of the slow time scale of lipid motion effectively restricting protein mobility, thus masking large-scale conformational drift that might provide evidence for an incorrect protein fold in the model. To evaluate this we ran a longer simulation in a lipid bilayer than before (i.e., K3W13, 10 ns, and K3W20, 5 ns) but also examined behavior of the model in octane where we believed that the faster motions of the octane would allow the protein model to sample more conformational space within the simulation time (10 ns). As seen above (Figure 3), the transmembrane secondary structure elements do not show further drift of secondary structure elements in the 10 ns bilayer simulation beyond that which occurs in the first 1 ns. Similarly, despite the more fluid nature of the octane, there was not a significant increase in protein motions within the TM regions. There was an increase in fluctuation of regions exposed to the water, possibly arising from the sharper interface between the solvent and the "membrane".

2. PME vs Cutoffs. As mentioned above there has been some discussion of the relative merits of cutoff vs PME methods for treatment of long-range electrostatic interactions in membrane

simulations.[75,76] In particular, it has been suggested that the way in which such interactions are treated may be expected to result in differences in the motion of ions and water through the filter. However, in the current study, concerted movement of ions and water was in both the cutoff and PME simulations. Also the use of PME did not significantly alter the overall conformational stability of the system (as measured by the Cα-RMSD) and did not appear to alter either inter- or intrasubunit interactions.

4.2. Simulation Methodology. It is useful to attempt to assess the limitations of this work. First, it is important to remember that the channel model is an incomplete representation of Kir6.2, with truncated termini (see refs 33 and 77 for further discussion). There are also limitations to the simulation protocol. Limitations of the force field include: (i) use of united atoms (rather than explicit hydrogens) for hydrocarbon groups; and (ii) use of single point charges rather than a polarizable force field, especially for water molecules and/or carbonyl groups interacting with ions. Both of these aspects may benefit from further study. There is also the problem of computational restrictions upon the time scale of these simulations. In part we have addressed this by using octane as a (more fluid) bilayer mimetic, and by running an extended simulation (10 ns) of Kir6.2 in a bilayer in order to examine protein dynamics on a time scale approaching that of biological interest. We note that ca. 10 ns is of the same order of magnitude as the time for a *single* K^+ ion to pass through a channel.

4.3. Biological Relevance. There are two aspects of biological relevance we wish to address: (i) whether a model of the Kir6.2 transmembrane domain can be realistically modeled on the X-ray structure of KcsA; and (ii) how the filter may change its local conformation to accommodate K^+ vs Na^+ ions, both of which can pass through the Kir6.2 channel.[77]

There has been some discussion[78,79] of the best model for the Kir6.2 transmembrane domain, and in particular as to whether the fold of this domain is significantly different from that of the bacterial channel KcsA. If the latter were true then it would not be reasonable to use KcsA a template upon which to base a homology model of Kir channels. The simulations reported here all give low Cα RMSDs for the KcsA-based model of Kir6.2, revealing a degree of backbone drift comparable to that seen in simulations that started from an X-ray structure.[25,55] Thus, they do not provide any evidence in favor of inherent "instability" of a KcsA-based model of a Kir channel. Furthermore, recent bioinformatics studies[80] have revealed a bacterial homologue of Kir channels which is homologous to *both* mammalian Kir channels *and* to KcsA. This also supports use of KcsA as a template for Kir6.2. We have recently compared one of the current simulations (K3OCT) with a simulation under similar conditions but using a model based on the sequence alignment of.[78] The latter simulation gave a significantly higher structural drift[34] than that in K3OCT, further supporting the KcsA-like model of Kir6.2 used in the current study, as does a recent experimental study.[35]

Turning to ion permeation, our simulations reveal single file concerted motion of ions with water along the selectivity filter both for K^+ and for Na^+ ions. The former has been seen in a number of K channel simulations.[21,23,25] For both ionic species the filter is seen to be flexible as the ions and water move through it. This suggests that the earlier proposal of K^+ selectivity arising from a rigid pore providing an exact fit to the K^+ ions[24,30] may be something of an oversimplification. This is in accord with a number of experimental studies that demonstrate that Na^+ ions may permeate K channels in the absence of competing K^+ ions.[81−83] Furthermore, recent X-ray studies of KcsA at a higher resolution have provided evidence for a degree of conformational flexibility of the filter.[27] This element of convergence between X-ray studies (at a temperature of 100 K) and simulation studies (at 300 K) is encouraging in terms of the ability of the latter to yield meaningful and new information.[84]

Our simulations indicate that Na^+ has a distinct form of binding in the filter region, exhibiting an octahedral coordination at S4, as opposed to the distorted cubic coordination preferred by K^+. Furthermore, the filter was able to narrow slightly to allow optimal liganding of the smaller Na^+ ion in S2. It is possible that the replacement of the Y residue of the filter region GYG motif of KcsA (which has a low permeability for Na^+) by an F residue in Kir6.2 (which has an appreciable permeability for Na^+) might facilitate such flexibility of the filter due to the loss of H-bonds to stabilize this region. This is supported by evidence that mutation of this Y to F or V in the Shaker potassium channel[85] and to L in Kv2.1[86] results in increasing Na^+ permeability. However,[87] were unable to identify any change in selectivity or permeability arising from a Y to F mutation in Kir2.1.

In summary, we have shown that multiple nanosecond MD simulations on a homology model of a mammalian K channel can provide useful insights into short time scale conformational dynamics of biological relevance. It is hoped that development and application of methods or addressing longer time scales in simulations will enable one to explore slower biological events such as channel gating.

Acknowledgment. Work in M.S.P.S.'s lab is supported by grants from the Wellcome Trust. C.E.C. thanks BBSRC for a studentship. Thanks to the Oxford Supercomputer Centre for computer time. Our thanks to all our colleagues for their interest in this work, especially Fran Ashcroft, Phil Biggin, Peter Proks, and Indira Shrivastava.

References and Notes

(1) Ghadiri, M. R.; Granja, J. R.; Buehler, L. K. *Nature* **1994**, *369*, 301.
(2) Engels, M.; Bashford, D.; Ghadiri, M. R. *J. Am. Chem. Soc*. **1995**, *117*, 7, 9151.
(3) Gallo, P.; Rovere, M.; Spohr, E. *J. Chem. Phys.* **2000**, *113*, 11324.
(4) Gordillo, M. C.; Marti, J. *Chem. Phys. Lett.* **2000**, *329*, 341.
(5) Murata, K.; Mitsuoaka, K.; Hirai, T.; Walz, T.; Agre, P.; Heymann, J. B.; Engel, A.; Fujiyoshi, Y. *Nature* **2000**, *407*, 599.
(6) Ren, G.; Reddy, V. S.; Cheng, A.; Melnyk, P.; Mitra, A. K. *Proc. Natl. Acad. Sci. U.S.A.* **2001**, *98*, 1398.
(7) Hille, B. *Ionic Channels of Excitable Membranes*, 2nd ed.; Sinauer Associates Inc.: Sunderland, MA, 1992.
(8) Roux, B. *Biophys. J.* **1999**, *77*, 139.
(9) Roux, B.; Bernèche, S.; Im, W. *Biochem.* **2000**, *39*, 13295.
(10) Goulding, D.; Hansen, J. P.; Melchionna, S. *Phys. Rev. Lett.* **2000**, *85*, 1132.
(11) Goulding, D.; Melchionna, S.; Hansen, J. P. *Phys. Chem. Chem. Phys.* **2001**, *3*, 1644.
(12) Jordan, P. C. *J. Gen. Physiol.* **1999**, *114*, 601.
(13) Boda, D.; Busath, D. D.; Henderson, D.; Sokolowski, S. *J. Phys. Chem. B.* **2000**, *104*, 8903.
(14) Nonner, W.; Chen, D. P.; Eisenberg, B. *J. Gen. Physiol.* **1999**, *113*, 773.
(15) Nonner, W.; Catacuzzeno, L.; Eisenberg, B. *Biophys J.* **2000**, *79*, 1976.
(16) Nonner, W.; Gillespie, D.; Henderson, D.; Eisenberg, B. *J. Phys Chem B* **2001**, *105*, 6427.
(17) Tieleman, D. P.; Biggin, P. C.; Smith, G. R.; Sansom, M. S. P. *Quart. Rev. Biophys.* **2001**. In press.
(18) Forrest, L. R.; Sansom, M. S. P. *Curr. Opin. Struct. Biol.* **2000**, *10*, 174.
(19) Roux, B.; Karplus, M. *Annu. Rev. Biophys. Biomol. Struct.* **1994**, *23*, 731.
(20) Sansom, M. S. P.; Shrivastava, I. H.; Ranatunga, K. M.; Smith, G. R. *Trends Biochem. Sci.* **2000**, *25*, 368.

(21) Åqvist, J.; Luzhkov, V. *Nature* **2000**, *404*, 881.
(22) Luzhkov, V. B.; Åqvist, J. *Biochim. Biophys. Acta* **2000**, *1481*, 360.
(23) Bernèche, S.; Roux, B. *Biophys. J.* **2000**, *78*, 2900.
(24) Allen, T. W.; Kuyucak, S.; Chung, S. H. *Biophys. J.* **1999**, *77*, 2502.
(25) Shrivastava, I. H.; Sansom, M. S. P. *Biophys. J.* **2000**, *78*, 557.
(26) Bernèche, S.; Roux, B. *Nature* **2001**, *414*, 73.
(27) Zhou, Y.; Morais-Cabral, J. H.; Kaufman, A.; MacKinnon, R. *Nature* **2001**, *414*, 43.
(28) Perozo, E.; Cortes, D. M.; Cuello, L. G. *Nature Struct. Biol.* **1998**, *5*, 459.
(29) Doupnik, C. A.; Davidson, N.; Lester, H. A. *Curr. Opin. Neurobiol.* **1995**, *5*, 268.
(30) Doyle, D. A.; Cabral, J. M.; Pfuetzner, R. A.; Kuo, A.; Gulbis, J. M.; Cohen, S. L.; Cahit, B. T.; MacKinnon, R. *Science* **1998**, *280*, 69.
(31) Heron, L.; Virsolvy, A.; Peyrollier, K.; Gribble, F.; LeCam, A.; Ashcroft, F.; Bataille, D. *Proc. Natl. Acad. Sci. U.S.A.* **1998**, *95*, 8387.
(32) Ashcroft, F. M.; Kakei, M.; Kelly, R. P. *J. Physiol.* **1989**, *408*, 413.
(33) Capener, C. E.; Shrivastava, I. H.; Ranatunga, K. M.; Forrest, L. R.; Smith, G. R.; Sansom, M. S. P. *Biophys. J.* **2000**, *78*, 2929.
(34) Capener, C. E.; Sansom, M. S. P. *Eur. Biophys. J.* **2001**. In preparation.
(35) Lu, Z.; Klem, A. M.; Ramu, Y. *Nature* **2001**, *413*, 809.
(36) Sali, A.; Blundell, T. L. *J. Mol. Biol.* **1993**, *234*, 779.
(37) Ranatunga, K. R.; Kerr, I. D.; Adcock, C.; Smith, G. R.; Sansom, M. S. P. *Biochim. Biophys. Acta* **1998**, *1370*, 1.
(38) Adcock, C.; Smith, G. R.; Sansom, M. S. P. *Biophys. J.* **1998**, *75*, 1211.
(39) Davis, M. E.; Madura, J. D.; Luty, B. A.; McCammon, J. A. *Comput. Phys. Commun.* **1991**, *62*, 187.
(40) Guidoni, L.; Torre, V.; Carloni, P. *FEBS Lett.* **2000**, *477*, 37.
(41) Smart, O. S.; Goodfellow, J. M.; Wallace, B. A. *Biophys. J.* **1993**, *65*, 2455.
(42) Brovchenko, I.; Paschek, D.; Geiger, A. *J. Chem. Phys.* **2000**, *113*, 5026.
(43) Mezei, M.; Mehrotra, P. K.; Beveridge, D. L. *J. Am. Chem. Soc.* **1985**, *107*, 2239.
(44) Hermans, J.; Berendsen, H. J. C.; van Gunsteren, W. F.; Postma, J. P. M. *Biopolymers* **1984**, *23*, 1513.
(45) van Gunsteren, W. F.; Kruger, P.; Billeter, S. R.; Mark, A. E.; Eising, A. A.; Scott, W. R. P.; Huneberger, P. H.; Tironi, I. G. *Biomolecular Simulation: The GROMOS96 Manual and User Guide*; Biomos & Hochschulverlag AG an der ETH Zurich: Zurich, 1996.
(46) Hess, B.; Bekker, H.; Berendsen, H. J. C.; Fraaije, J. G. E. M. *J. Comput. Chem.* **1997**, *18*, 1463.
(47) Berendsen, H. J. C.; Postma, J. P. M.; van Gunsteren, W. F.; DiNola, A.; Haak, J. R. *J. Chem. Phys.* **1984**, *81*, 3684.
(48) Tieleman, D. P.; Berendsen, H. J. C.; Sansom, M. S. P. *Biophys. J.* **2001**, *80*, 331.
(49) Berger, O.; Edholm, O.; Jahnig, F. *Biophys. J.* **1997**, *72*, 2002.
(50) Marrink, S. J.; Berger, O.; Tieleman, D. P.; Jahnig, F. *Biophys. J.* **1998**, *74*, 931.
(51) Straatsma, T. P.; Berendsen, H. J. C. *J. Chem. Phys.* **1988**, *89*, 5876.
(52) Kraulis, P. J. *J. Appl. Crystallogr.* **1991**, *24*, 946.
(53) Merritt, E. A.; Bacon, D. J. *Methods Enzymol.* **1997**, *277*, 505.
(54) Kabsch, W.; Sander, C. *Biopolymers* **1983**, *22*, 2577.
(55) Tieleman, D. P.; Berendsen, H. J. C. *Biophys. J.* **1998**, *74*, 2786.
(56) Sansom, M. S. P.; Bond, P.; Beckstein, O.; Biggin, P. C.; Faraldo-Gómez, J.; Law, R. J.; Patargias, G.; Tieleman, D. P. *Novartis Foundation Symposia* **2001**, *245*. In press.
(57) Smart, O. S.; Neduvelil, J. G.; Wang, X.; Wallace, B. A.; Sansom, M. S. P. *J. Mol. Graph.* **1996**, *14*, 354.
(58) Smart, O. S.; Breed, J.; Smith, G. R.; Sansom, M. S. P. *Biophys. J.* **1997**, *72*, 1109.
(59) Tieleman, D. P.; P., S. M. S. *Int. J. Quantum Chem.* **2001**, *83*, 166.
(60) Yau, W. M.; Wimley, W. C.; Gawrisch, K.; White, S. H. *Biochem.* **1998**, *37*, 14713.
(61) Killian, J. A.; von Heijne, G. *Trends Biochem. Sci.* **2000**, *25*, 429.
(62) Cortes, D. M.; Cuello, L. G.; Perozo, E. *J. Gen. Physiol.* **2001**, *117*, 165.
(63) Shrivastava, I. H.; Capener, C.; Forrest, L. R.; Sansom, M. S. P. *Biophys. J.* **2000**, *78*, 79.
(64) Perozo, E.; Cortes, D. M.; Cuello, L. G. *Science* **1999**, *285*, 73.
(65) Green, M. E. *J. Phys. Chem. B* **2001**, *105*, 5298.
(66) Darden, T.; York, D.; Pedersen, L. *J. Chem. Phys.* **1993**, *98*, 10089.
(67) Essmann, U.; Perera, L.; Berkowitz, M. L.; Darden, T.; Lee, H.; Pedersen, L. G. *J. Chem. Phys.* **1995**, *103*, 8577.
(68) Chiu, S.; Clark, M.; Subramaniam, S.; Jakobsson, E. *J. Comput. Chem.* **2000**, *21*, 121.
(69) Weber, W.; Hunenberger, P. H.; McCammon, J. A. *J. Phys. Chem. B* **2000**, *104*, 3668.
(70) Allen, T. W.; Bliznyuk, A.; Rendell, A. P.; Kuyucak, S.; Chung, S. H. *J. Chem. Phys.* **2000**, *112*, 8191.
(71) Biggin, P. C.; Smith, G. R.; Shrivastava, I. H.; Choe, S.; Sansom, M. S. P. *Biochim. Biophys. Acta* **2001**, *1510*, 1.
(72) Burgess, J. *Ions in Solution−Basic Principles of Chemical Interactions*; Ellis Horwood Ltd: Chichester, 1988.
(73) Krestov, G. A.; Novosyolov, N. P.; Perelygin, I. S.; Kolker, A. M.; Safonova, L. P.; Ovchinnikova, V. D.; Trostin, V. N. *Ionic solvation*; Pearson Higher Education: Harlow, 1994.
(74) Shrivastava, I. H.; Biggin, P. C.; Tieleman, D. P.; Sansom, M. S. P. *Biophys. J.* **2001**. Submitted for publication.
(75) Tobias, D. J.; Tu, K. C.; Klein, M. L. *Curr. Opin. Colloid. Interface Sci.* **1997**, *2*, 15.
(76) Tieleman, D. P.; Marrink, S. J.; Berendsen, H. J. C. *Biochim. Biophys. Acta* **1997**, *1331*, 235.
(77) Proks, P.; Capener, C. E.; Jones, P.; Sansom, M. S. P.; Ashcroft, F. *J. Gen. Physiol.* **2001**, *118*, 341.
(78) Minor, D. L.; Masseling, S. J.; Jan, Y. N.; Jan, L. Y. *Cell* **1999**, *96*, 879.
(79) Loussouarn, G.; Amkhina, E. N.; Nichols, C. G. *Biophys. J.* **1999**, *76*, A75.
(80) Durell, S. R.; Guy, H. R. *BMC Evolutionary Biology* **2001**, *1*, 14.
(81) French, R. J.; Wells, J. B. *J. Gen. Physiol.* **1977**, *70*, 707.
(82) Korn, S. J.; Ikeda, S. R. *Science* **1995**, *269*, 410.
(83) Loboda, A.; Melishchuk, A.; Armstrong, C. *Biophys. J.* **2001**, *80*, 2704.
(84) Sansom, M. S. P.; Shrivastava, I. H. *Curr. Biol.* **2002**, *12*, R65.
(85) Heginbotham, L.; Lu, Z.; Abramsom, T.; MacKinnon, R. *Biophys. J.* **1994**, *66*, 1061.
(86) Chapman, M. L.; Krovetz, H. S.; VanDongen, A. M. J. *J. Physiol.* **2001**, *530*, 21.
(87) So, I.; Ashmole, I.; Davies, N. W.; Sutcliffe, M. J.; Stanfield, P. R. *J. Physiol.* **2001**, *531*, 37.